Journal of Dynamic Behavior of Materials (2022) 8:20–38
https://doi.org/10.1007/s40870-021-00314-7

REVIEW ARTICLE

Advances in the Whipple Shield Design and Development:

A Brief Review

A. Pai[1] · R. Divakaran[1] · S. Anand[1] · S. B. Shenoy[1]

Received: 24 February 2021 / Accepted: 17 June 2021 / Published online: 20 July 2021

Abstract
Safety of satellites as well as spacecrafts during space missions is a primary objective to preserve the physical and virtual assets onboard. Whipple shields belong to the class of protective equipment provided on the surface of the spacecrafts and satellites, to sustain impacts from the ultra-high speed debris, which can otherwise cause considerable damage to the corresponding structures. Recent works on whipple shields are focussed on determining the response of different geometrical arrangements and material properties under hyper-velocity impact at projectile speeds of 3-18 km/s. Advances in the whipple shield design include integrated and mechanised models employing high performance materials like fiber-metal laminates ensuring better operational capability. The forward bumper of the whipple shield is the first line of defence as it regulates the state of projectile after the primary impact. Use of aluminium alloys for front bumpers is popular, owing to their lightweight and strength characteristics. The advances for the front bumper have seen usage of ceramic, metallic foams, and super composite mixtures, which resulted in enhanced performance, durability and safety of the whipple shields. This work is a comprehensive coverage of the latest materials used for whipple shields, their performance characterization—both experimental and theoretical, and applications.

Keywords Whipple shield · Hypervelocity impact · Space debris · Shielding materials · Satellite safety

Introduction

Space debris and meteoroids cause a potent risk to space operations as a result of hyper-velocity impacts in the lower orbit [1–3]. Space debris can be classified as objects of variable size, in trajectory, with man-made or foreign (from outer space) origins. It comprises of old and inactive satellites, the discarded stages of rockets, additional unwanted materials such as fasteners and instrumental covers separated from their parent structure, and remnant fragments of asteroids, comets that enter the earth's atmosphere as meteors or meteorites [4]. Debris also comprises of wreckages of vehicles that are shattered or crashed, and waste components that are shed off from satellites like linings [4]. The number of orbital debris objects which are tracked by space surveillance network exceeds 28000, the untracked space objects exceed 29 million [5]. The large variability in the size account for multiple challenges in designing whipple shields. Space debris can be as large as a large rocket and can scale down to tiny micro-particles. As per ESA's annual report [5], the size distribution of the space debris is shown in Fig. 1 . If the space debris damage the systems critical to the satellite flight, a catastrophic failure can occur leading to a cascading effect on the operations side. Thus, safe and reliable design of satellites or any spacecraft encountering the impact scenarios is vital for missions in earth-orbiting and geo-sensing. The response of spacecraft/ satellite structures to impact became a significant issue for the design of whipple shields [6]. In future, the heavily populated orbit with

✉ S. B. Shenoy
satish.shenoy@manipal.edu

A. Pai
anand.pai@manipal.edu

R. Divakaran
raghuvaran27d@gmail.com

S. Anand
shlokanand93@gmail.com

[1] Department of Aeronautical and Automobile Engineering, Manipal Institute of Technology, Manipal Academy of Higher Education, Manipal 576104, India

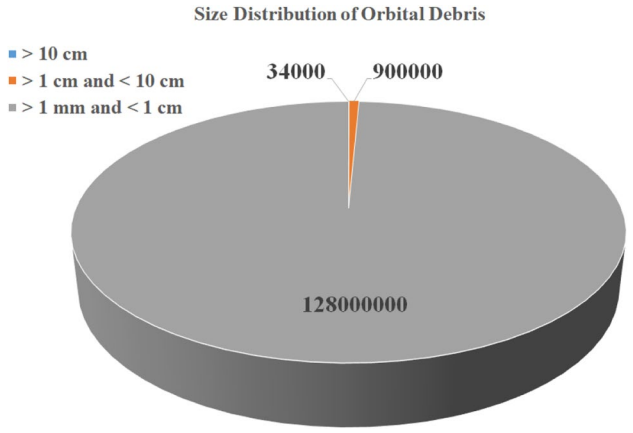

Fig. 1 Size distribution of space debris [5]

satellites and debris pose the threat to newer launches creating a dire need for stringent shields against imminent impact.

In order to tackle the impact caused by space debris travelling at hyper-velocities, Fred Whipple invented the "Whipple shield" in the 1940s [2]. Whipple shields are low-weight shielding barriers which need to withstand hypervelocity impacts (shown in Fig. 2) and meteoroid hits. It comprises of a thin external bumper located at a uniform space from the core spacecraft barrier. The bumper is used to distribute the kinetic energy of the impacting object among the layers between the wall and the bumper. The hypervelocity range for the orbital debris and micrometeoroids lies between 3 and 18 km/s. Whipple shields have found significant applications in the space vehicles. The DESTINY module of the ISS (International Space Station) utilized high strength fabrics to shield itself from getting damaged by the orbital debris impact [6]. The arrangement of the module whipple shield consisted of the high-strength fabric placed between the outer aluminium bumper and the exterior wall.

The Whipple shield configurations have seen constant transformation over the years- one such being employment of a stuffed Whipple shield comprising a porous, light-weight layer like a foam (metallic or polymer), in between the rigid layers of the shield [7]. This configuration results in lesser chances of penetration. Another variant is a Multi-shock shield consisting of several bumpers aligned in a specific geometry to maximize the protection against impacts [8]. This review covers the use of advanced materials in construction of whipple shields, the novel configurations used to withstand hypervelocity impacts and the development in the testing methods for assessing the performance of the various designs. Figure 3 shows the chronology of the research in the past 30 years on whipple shields.

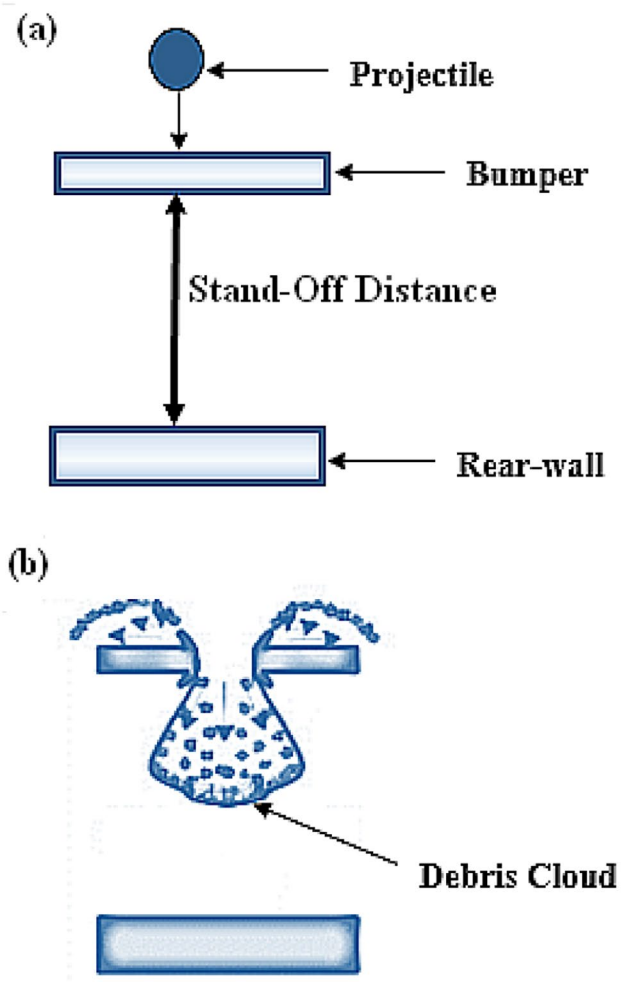

Fig. 2 **a** Whipple shield configuration, **b** Impact on whipple shield due to space debris

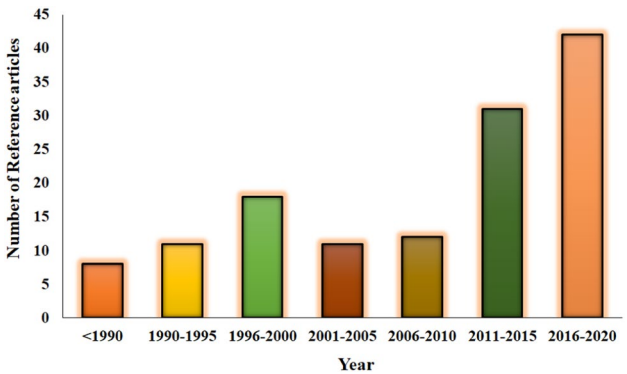

Fig. 3 Chronological distribution of the research on whipple shields

Methodology

Construction of Whipple Shields

Whipple shields consist of a thin (relatively) outer wall to fragment incoming micrometeoroids and debris, and fan it out. For the facing material, metallic sheets were popular in initial designs of the 1990s [3, 9], while in later designs, ceramic facet layers were employed [10, 11]. Ceramics being hard and brittle, withstand the impact by sacrificial fragmentation leading to a phenomenon known as "Mushrooming" [10]. A combination of ceramic matrix composites (CMCs) and metal matrix composites (MMCs) produced by the powder metallurgy, would be very promising for use as facet materials. For the consequent layers of the whipple shield, metal foams, and super composite mixtures were utilized [12]. In capacity of the facet material, Aluminium and its alloys such as AA6061-T6, AA2024-T3, AA2017-T4 [13] were popular owing to their high strength-to-weight ratio, favorable deformation mechanics [14]. Table 1 shows the popular aluminium alloys in use as whipple shield materials.

B_4C possesses low density and greater hardness when compared to other ceramic materials, but the limited toughness and the high cost hinder its popular utilization. For increasing the toughness while reducing cost, B_4C ceramic and other metallic materials (such as Ti, Mg, Al, Cu) are used in combination in CMCs. The B_4C/Al composite has similar, even lower density when compared to conventional aerospace Al alloy, and its hardness and modulus are higher [15]. The toughness of B_4C/Al composite is observed to be much better than B_4C stand-alone ceramic layer. Hence, B_4C/Al composite as a new bumper material has high potential in MMOD shield models. In some configurations, materials with high thermal resistance and excellent mechanical properties such as Nextel/Kevlar™ [16, 17] were used as succeeding fabric layers after the bumper for stalling the hypervelocity debris.The properties of common alloys used in space applications is shown in Table 2.

Theoretical and Experimental Analysis of Whipple Shield Configurations

Owing to the complexity, high cost and hazards involved in the hypervelocity setup for experimentation, researchers have resorted to theoretical approach in analyzing the effectiveness of whipple shields under such impacts [18, 19]. Both numerical and analytical techniques were developed for this analysis.

Numerical Simulation

There were several numerical simulation techniques such as artifical neural networks (ANNs), AUTODYN-2D, multi-material model, solid mechanics code (CTH), and smoothed particle hydrodynamics (SPH) available to assess the performance of different whipple shield configurations. The influence of key factors like the impact velocity, projectiles

Table 1 Common aluminium alloys used in whipple shields

Alloys	Features
AA2024	High strength-to-weight ratio, "Cu" key element
AA5052	Highest strength alloy for non-heat-treatable grades, highly malleable
AA6061	Heat-treatable with high strength
AA6063	Excellent finish properties, useful in anodizing
AA7050	Corrosion resistant, durable than AA7075, fracture and corrosion resistant
AA7068	Strongest alloy of aluminium, corrosion resistant
AA7075	Strength comparable to steel, good machinability and fatigue strength

Table 2 Material properties of materials used in space applications [16, 79]

Material	Tensile strength (MPa)	Yield strength (MPa)	Young's modulus (GPa)	Thermal conductivity (W/m-K)	Coeff. of thermal expansion (μ m/m-K)
Al-2024-T3	483	345	73.1	121	23.3
Al-6061-T6	310	276	68.9	167	23.6
Al-2017-T4	427	276	72.4	134	23.6
SUS 304	505	215	200	16.2	17.3
Titanium	240	310	105	16	8.6
Al/Mg	280	180	45	125	26

size and shape, impact trajectories, on the whipple shield response were studied by different researchers [7, 20–22]. In 1995, Katayama et al. [23, 24], conducted numerical simulation on the Whipple shield through the impacts caused by the space debris for impact velocity of 10 km/s and in 1997, the analysis was extended for varying impact velocities (for 2, 4, 7 km/s) . In this work, three types of projectiles and accelerators were considered and varied with three different stages i.e., powdered gun for the first stage, light-gas gun for the second stage and rail gun for the third. 2D hydro code was used to analyse the effects caused by the hypervelocity phenomena. Both lagrangian and eulerian description were used to describe the fundamental equations for the conservation of energy, momentum and mass for the Whipple shields at the central stage and for single target analyses, with the final stages respectively. In contrast to the eulerian approach, the lagrangian method yields a material limit that could determine the rate of the debris cloud growth and pertinent impact on the main wall [25]. However, with the Eulerian method, the researchers were able to achieve the complete simulation effect during impact deprived of complex physical process involved with the space debris. [24]. In 1993, Christiansen et al. [26], studied the functioning of different shields against the meteoroids and space debris, for which an equation series was proposed. The simulations were conducted at the Hyper-Velocity Impact Test Facility at the NASA Johnson Space Centre. The Multi shock shielding with high strength material Nextel [27] and Double-Mesh Bumper shield,were performed under hyper-velocity impacts. From this work, the BLE along with different sizing for a combination of material properties were obtained.

An alternate method to achieve the simulation of hypervelocity impact is the Artificial neural network (ANN), a computing system comprising different neurons that maintain their interconnections to retain memories or relations implicit within a data environment. These switches, or neurons, are simple computational nodes that evaluate an input vector against a thresholding function and provide a single output [28–30] as seen in Fig. 4. Ryan et al. [30] have used a multi-layer perceptron architecture in their analysis of hypervelocity impact vis-a-vis the interaction between the aluminium projectile and aluminium whipple shields. For the input exemplars, projectile and target parameters were chosen, while for the output, the target damage measurements or penetration depths/ perforation profiles were selected. The study revealed some critical inputs, like the rear wall thickness, the projectile velocity and shield standoff. Additionally, unexpectedly important inputs like the projectile tensile modulus, bump linear coefficient of thermal expansion, rear wall electric resistivity were also identified [30]. Along the lines of ANN, support vector machines (SVM) were utilized for analysis of whipple shield performance. SVMs are popularly used in data mining and machine learning application with sparse data sets [31].

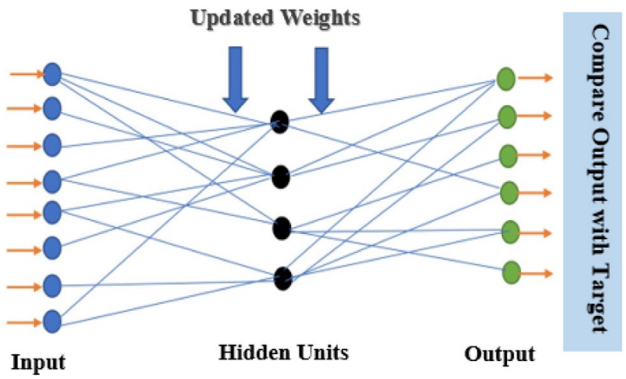

Fig. 4 Representation of the neural network

Commercially available software "Autodyn" has been used for the hypervelocity impact simulation, which consists of a variety of tools, with the adaptability to use lagrangian elements for solids and eulerian ones for liquids. Lagrangian, Eulerian and multi-material Euler solvers have been used in recent research for obtaining the explicit results [21, 32, 33]. The inbuilt auto communication between the solvers could incorporate the relation model for erosion, blast and impact simulations when subjected to hypervelocity events.

Alternately, Smoothed particle hydrodynamics (SPH) is a model of computing systems used for a mechanical simulation such as mechanics of solids and fluid flow which comprises a mesh-free lagrangian method [20, 34]. SPH shows benefits in terms of the change in coordinates with the fluid flow, for evaluating the flow properties irrespective of the spatial variation. Due to its considerable merits, SPH method was adopted and made functional for computation of high deformation mechanisms of materials. Additionally, algorithms were presented for axis-symmetric models. The distinctiveness of the cylinder-shaped SPH hydro code was advanced for mutual migration between the coordinate systems. SPH calculates pressure with assistances of weight from adjacent elements relatively than by resolving system of linear equations. Lastly, unlike grid-based systems which is limited by the trajectory of fluid flow, SPH generates an unrestricted surface for two phased fluids as the particles represent high density fluid like water and low-density fluid represented in empty space. Groenenboom et al. [35] discussed the advantages of SPH method in simulating the hypervelocity impacts (HVI) for 2D and 3D models in contrast with conventional FE methods. In 1993, Chhabildas et al. [36], conducted a sequence of tests to estimate the efficiency of Whipple shield (WS) bumper against the space-debris travelling at 10 km/s. Simulations were carried out for 19 mm and 12.7 mm flier-plates, accomplished via multidimensional hydrodynamic code CTH. The complete perforation of the sub-structure by the consequent debris cloud were

computed. The results stated that for 19 mm flier-plate, fragmentation of the aluminium (Al) shield bumper was caused leading to its disintegration. In 1995, Alme et al., [37] presented a scaled result on the basis of CALE hydrodynamics code simulations of aluminium projectile effects on classic aluminium whipple shields. The range of projectile sizes and melting temperatures of the target material were computed. The computational simulations for variable impact speeds from 6 to 14 km/s, coupled with variation in the areal densities from 5 to 80%. The projectile diameters was fixed at 19 mm weighing 1.27 g. The specific kinetic energies were compared with the heat content required for achieving the melting of the shield materials as per the Hultgren-Table [38]. Those materials having an enthalpy of fusion lesser than the specific kinetic energy of the projectile melted completely, while partial melting was observed for the materials having the enthalpy of fusion higher than the specific kinetic energy of the projectiles. In the same year, Fahrenthold et al. [39] presented a model of debris cloud growth for applications in oblique hyper-velocity impacts employing ALE

Table 3 Details of the setup for hypervelocity impact simulation

Researchers	Numerical simulation method	Impact velocity (km/s)	Key observations	Additional parameters
Rabb [40]	SPH	3	Slight bulge-1mm deep [Dia-2mm], Spallation [Dia-3mm]	Impact angle
Katayama [23]	AUTODYN-2D	4	Spallation, pedalling, ductile fracture	Density
Fahrenthold [40]	SPH	5	Slight bulge-1mm deep [Dia-3mm], Spallation, bulge-2mm deep [Dia-4mm]	Critical particle diameter
Hiermaier [33]	AUTODYN-2D	5.1	Surface crack/no perforation	Pressure
Cour palais [41]	-	6.25	Perforated; partial tear; 6 cm spall	Momentum
Kerr [42]	CTH	7	Rear-wall perforation	-
Christiansen [26]	-	8	25% damage threat (perforation)	Impact angle
Palmieri [43]	PAMSHOCK	9.5	No Perforation	Stress
Chhabildas [36]	CTH	10	Bumper Disintegrates into debris cloud	Mass threshold
Taylor [44]	AUTODYN/SPH	11.19	Al-1100 failure stress	Pitch and yaw
Palmieri [43]	PAMSHOCK	12	Perforation	Stress
Palmieri [43]	PAMSHOCK	13	No perforation	Stress
Williamsen [45]	SPH	14	Perforation	Momentum multiplication factor(k)
Zhang [46]	SPH	6.7	Critical penetration analysis and critical impulse analysis conducted	Particle position/velocity analysis
Bjorkman [47]	NASA-JSC BLE	2.27-7.2	Detached spall failure and Perforation compared	Shock enhancement approach and debris cloud cratering model
Piekutowski [48]	NASA-JSC BLE	6.94-9.89	Detached spalls on the rear walls	Shield melting and incipient vaporization
Wen [49]	SPH, Grady Spall Model	2.23-5.26	Fragment location, velocity, and mass compared with perforation test results	Radial position mapping of fragments
Kerr [42]	CTH	14.5	Rear-wall perforation	-
Horner [50]	Eulerian adaptive-mesh hydrodynamic	18	The bumper is perforated by the projectile. Survives, no perforation, and no incipient spall	Density
Carrasquilla [7]	CTH	5.06-6.61	Ellipsoid projectiles simulation agreed with experimental HVI results	Shaped projectiles
Tjønn [51]	IMPETUS Afea Solver	3-5	Model sensitivity to plate thickness, impact velocity, material density	Size and origin of orbital debris
Liu [52]	SPH for non-prestress film and AUTODYN for pre-stress film	2.9-5	Ductile penetration (in the central impact zone) and brittle cracks damage (in the non-impact zone)	Length and direction of crack formation

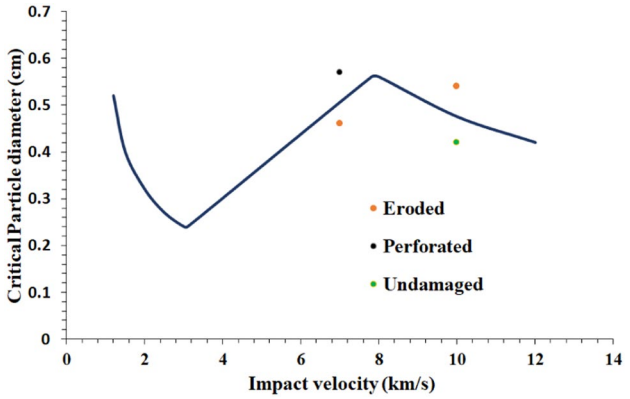

Fig. 5 Ballistic limit curve observed in [39]

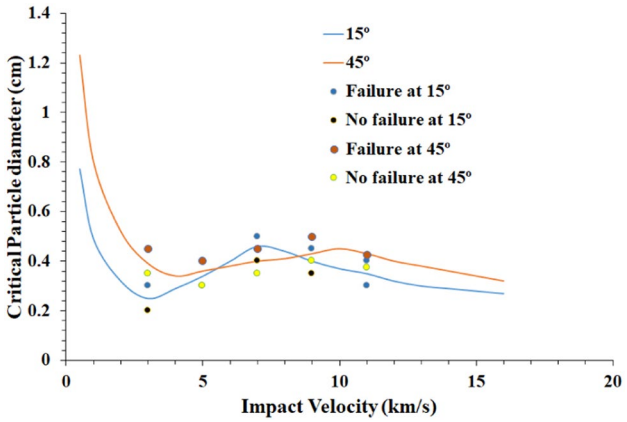

Fig. 6 Ballistic limit curve observed in [40]

codes in the simulation runs using DYNA3D and CTH. The limitations of the non-uniform densities and void spaced distributions in previous models were overcome in the current model (Refer Fig. 5). The current code possessed better competence for inexplicit impact analysis. Table 3 shows the setup used for different simulation studies of HVI.

In 1997, Kerr et al. [53], simulated the hyper-velocity impact on whipple shields using an oblique-impact angle of 30°. The simulation results were compared with the hyper-velocity impact tests. An Al-Al impact at 5 km/s resulted in a debris-cloud comprising primarily of large "chunky" fragments [54]. Additionally, simulations were carried out on the whipple shield for velocity-regime beyond 8 km/s. Various issued BLEs were used for validating the consistency of the equations. In 1998, Hayhurst et al. [17] used numerical techniques to simulate a bumper shield being impacted by projectiles at hyper-velocities. The simulation consisted of normal and oblique impacts on the aluminium bumper shields. These results were validated using experimental results. After the test of aluminium shields, Nextel and Kevlar-epoxy shields were also simulated. In 1999, Rabb et al. [40], performed a sequence of simulations based on 3-D hybrid-particle finite element coding technique. This study carried out dual set of oblique impact-simulations for a single-bumper WS and for a WS with double bumper or stuffed-WS whose results are compared to issued BLEs (Fig. 6). In conclusion, the results specify that the 3-D hybrid-particle finite element coding technique is capable ofproviding higher accuracy results and it is computationally controllable method to carry out simulations in order to study the performance of the space debris shielding.

In 2001, Palmieri et al [43], used AUTODYN-2D and PAMSHOCK-3D in order to determine the normal ballistic impact curve for an Al-spaced WS by varying velocity from 7 to 15 km/s. The results of AUTODYN-2D were compared to the NASA ballistic-limits (Range 7-11 km/s). It was observed that the NASA ballistic-limit curve showed a drop in curvature and AUTODYN-2D showed an increasing curvature at higher velocities. The PAMSHOCK-3D calculations overestimated the two curves for velocities between 7 and 13 km/s. Both the codes predicted accurate results for the two shielding materials for with and without perforation using light-gas gun experiments till 7 km/s. Although, AUTODYN-2D was able to predict the maximum depth of crater for cases with no perforation. In 2001, Taylor et al., [44] conducted 56 numerical simulations using SPH in order to study the effect of hollow-shaped charged jet projectile against the stuffed whipple shields. The projectile was modelled hydro-dynamically, to reflect the material state. Nextel/Kevlar epoxy-bumper was modelled as a substitute to aluminium with the same thickness. The debris cloud's structural morphology comprising the projectile's form, yaw, strength and pitch at velocity of 11 km/s was analyzed in detail. The provisional bumper was seen to fail due to ejection of fragments travelling at velocity of 2 km/s. Subsequently, it was also seen that the rear-wall was distorted by the fragments with no perforation. In 2003, Hiermaier et al., [33] conducted simulations to study the ellipsoid projectile effect on whipple shields using AUTODYN- 2D and AUTODYN-3D. The simulation results were compared with the experimental results from the impact studies of a two staged light-gas gun. Al-alloys were considered as the materials for both the target and the projectiles. Three kinds of projectile shapes - prolate, oblate and sphere were studied. The mass of the projectiles were maintained constant at 0.183 g. The configuration of the whipple shield comprised a 200 mm standoff core, 1 mm thickness of the bumper-shield, with back-wall thickness of 3 mm. Impact velocities ranged from 0.85 to 10 km/s.

In 2008, Buyuk et al [21], combined the analytical hydro-code simulation with approximate-optimization method. Successive-design method was used to determine the extreme conditions for the modelled WS focusing on

variation in the orientation and shape of the projectiles by limitating the total-projectile mass along with radar cross-section (RCS). Non-linear explicit dynamic numerical-solver LS-DYNA and LS-OPT were used to conduct the Hyper-Velocity impacts simulation and response-surface methodology was used for optimization. Additionally, SPH and Coupled-finite element parametric modelling were conducted. It was reported that the projectiles with dissimilar shape and orientation produce more risk compared to typical spherical-projectile with similar RCS and mass. In 2008, Horner et al. [50], analysed the response of the shielding systems employing the Cour-Palais and Christiansen BLE [[27]] and compared it with the results obtained from adaptive mesh-eulerian hydrodynamic codes, based on the Mie- Gruneisen mechanics of solids [55]. The projectiles used were 1 mm-sized iron/nickel (Fe/Ni) spheres. Shield-thicknesses estimated by the Cour-Palais/Christiansen BLE were consistent with those yielded by the hydro-dynamic modelling. In 2008, Kerr et al., [42] conducted a sequence of 14 hypervelocity impact tests utilizing the CTH-hydro code. The model consisted of a spherical aluminium, double-bumper whipple shield, impacted at 7 km/s. The ballistic-limit curves were developed for the whipple shield configurations. Primary CTH-hydro code simulations were performed at the Hyper-Velocity Impact Test Facility, NASA-Johnson Space-Centre. The studies showed that the diameter of the spherical whipple shield had to be large compared to that of the flat plate whipple shileds by an aspect ratio of 2.2 for 7 km/s and 1.6 for 14.5 km/s for the same extent of damages. In 2008, Schonberg et al., [56] determined determined the critical diameter of projectile for hypervelocity impacts and incroporated it into the NASA-JSC ballistic limit equation which reduced the mass by almost 52 %. A flaw in the NASA-JSC Ballistic limit equation was identified for oblique impact angles beyond 60°. In 2009, Bohannan et al. [57] simulated a shear-thickening fluid treated Kevlar in stuffed whipple shields, for hypervelocity impact performance. The membrane particle-element methods gave reliable results for perforation and fragmentation for stuffed Whipple arrangements. In 2011, Hussain et al. [58] used hydro codes to evaluate the penetration characteristics of explosively formed projectiles. The projectiles were hurled against a spaced armour with multiple whipple shields to arrive at the configuration with the lowest weight that displayed good tolerance against the impact. In 2012, Hussain et al. [59] studied the fragmentation mechanism of the projectiles in form of shaped-charges on impact with the whipple shields designed for light armour vehicles. Numerical simulations showed that the shield with thickness of 0.75 mm was the most effective against the shaped-charges. In 2013, Ryan et al., [60] used an artificial neural network (ANN) in order to calculate the perforating effect boundaries of aluminium whipple shield subjecte to hypervelocity impact. Based on the material input properties, geometry of the whipple shield and conditions due to impact, a multilayer perceptron (MLP) was developed. The network output was an equivalent probability function of the perforating effect, with a sigmoidla fit between the perforating and non-perforating experimental effects. Skeletonization was conducted on the network. From the test, the effect of the traditional constraints like thickness of the rear wall, velocity of the projectile, stand-off distance of the shield were verified. The unpredictably significant constraints such as rear wall electrical resistivity, projectile tensile modulus were also highlighted from the test. The design delivered precise success/failure calculations for 92% of test runs. In 2014, Zhang et al. [61], proposed a modified SPH method capable of faster numerical simulations for hypervelocity impact studies of whipple shields. One of the factors considered for the rear-wall penetration was the specific impulse. In this study, focus was given to the critical specific impulse rather than the critical-penetration. Based on the secondary debris isotropic-expansion concept, the specific impulse study was transformed to spatial and velocity vectors of the particles leading to a reduction in the space span and the physical-evolution time of the model.

In 2016, Zhang et al. [62], studied the use of egg-box panels in whipple shields. The flat-panels in the whipple shields were replaced by the egg-box panels of similar areal density. The effect of the different factors- area of impact, size of the cell, and axial-offset were studied. The degree of fragmentation was lower in the case of the egg-box panels. In 2017, Carrasquilla et al. [63], conducted a numerical analysis to determine the effects of different shapes of aluminium projectiles on dual wall shields using CTH. Three numerical simulations were performed and the results were compared with the EMI test results. The BLE was found to be improved for prolate ellipsoids and it remain unchanged for spheres, especially at small impact velocities. The velocities for the iterations were vaired between 4 and 8 km/s. Beyond 8 km/s, the phase change from solid to liquid/vapour constrained the analysis. In 2017, Silnikov et al. [34], studied the effect of orbital debris on the fragmentation of structures under hypervelocity impact. A numerical model was developed based on the SPH technique, LS-DYNA was used for the simulations. The results from numerical simulation were compared with experimental results for a spherical, cylindrical and cubical shapes of projectiles impacting a thin-plate. For the cubical projectile, the edge impact led to the formation of a high-density debris cloud detrimental to the shield structure. In 2017, Williamsen et al. [45], estimated the momentum improvement (K-factor) for the space debris impact onto dual-wall shielding systems. A SPHC hydrocode was used for simulating successive, normal as well as oblique impacts on the shields. The factors considered were the computational time, size of the plates and angle of impact. In 2017, Jing et al. [64], explored the aerogel/

fiberglass composite stuffed shields for spacecraft applications. Emphasis was given to the thermal response of the shields. Comparison was drawn between the stuffed shields and triple aluminium shields, which showed superior performance of the stuffed shields in withstanding the thermal loads.

The size of the particles in the debris cloud play an important role. Large sized debris are traceble while mm-sized debris are not which pose a higher risk of imminent impact with the space vehicles. In 2017 Deconinck et al. [65] carried a numerical study of the impact of small sized debris on honeycomb sandwich structures. The numerical results were validated by the experiments conducted at the Thiot Ingenierie Shock Physics Laboratory. In 2018, Pydah et al. [66] analyzed the transient elasto-plastic deformation in a dual-core sandwich shield. The core was made of high strength steel. The core geometry considered were honeycomb and Miura-ori celled. A combination of honeycomb and Miura-ori core showed the least deflection.Of late, Ceramo-aluminium sacrificial bumpers are being used for the outer layer of the whipple shields. In 2018, Cherniaev [10] constructed such bumpers based on shock impedance matching. The hypervelocity impact simulation was carried out using the hydro code modelling. In 2019, Putzar et al. [67], performed nine effective hypervelocity impact tests on two-layered and a three- layered shields. A new BLE was proposed for the three-layered shield and was compared to the CAST BLE. Similarly, on comparing the two layered shields to the Christiansen Whipple shield BL equation for velocities between 7.1 and 7.9 km/s, the layered shields were inferior to all-aluminium shield, having the same surface densitiy. The poor fragmentation at the bumper led to the reduction in the performance. Similarly, impact craters were evident on the rear wall at 7.94 km/s, which suggest that the transitional velocity were above 7 km/s for the bumper. In 2020, Zhao et al. [14] identified that fibre fabric and fabric-reinforced polymers experience shock compression and fragmentation under hypervelocity impact. The fabric-only bumper shield gave inferior results during the simulations, when compared to the all-aluminium bumper configuration. The model was extended to hybrid fabric-reinforced polymer/aluminium shields which reduced the shock peaks under hypervelocity impacts and produced large deformation to absorb the kinetic energy of the projectiles. In 2020, Wen et al. [49] related the fragmentation conditions cto the type of damage endured by the rear wall of whipple shields. 20 different whipple shields underwent hypervelocity impact tests and the damage endured by the rear wall was compared to the fragmentation pattern.

Table 3 compares the different numerical techniques used for simulating hyper-velocity impacts. SPH, CTH PAMSHOCK, and AUTODYN were the popular simulation techniques, employing key metrics of impact velocity, impact angle, critical particle diameter, momentum, pressure, density and mass threshold. The effect of the impact in terms of the bulge size and depth, perforation location and extent were studied in detail.

Experimental Analysis of Whipple Shields

To understand the physical response of whipple shields to hypervelocity debris, the experimental setup consisted of a multi-stage gas gun which could shoot projectiles of different sizes and shapes at velocities at very high magnitudes. The whipple shield response to the impact could shed light on the probable defensive capability of the material against the debris cloud in the outer space. In the year 1990, Christiansen [2] conducted an experiment in collaboration with the Hypervelocity Impact Research Laboratory to test out different materials and arrangements to develop an advanced shielding system. Some of the materials tested were metallic, ceramic or composites. Among the tested candidates a multi-shock model (Cour-Palais et al. [68]) and a double bumper arrangement of aluminium meshes with epoxy composites was observed to have the best performance. All the comparisons were done a conventional Whipple shield aforementioned.

In 1995, Cour-Palais et al., [41] studied the response of low-melting projectile materials like cadmium (Cd), for hypervelocity impact on space shields. Based on the proposed design by Morrison et al. [69], the experiments were conducted. Cadmium projectiles at hypervelocities were used to impact Aluminium and Multi-Nextel™ ceramic bumper shields. The studies were carried out at the University of Dayton Re-Search Institute. The shields were able to withstand impacts upto the velocities of 8.3 km/s.

In 1997, Lambert et al. [70] compared shields made of aluminium, Kevlar and glare using hypervelocity impact experiments. The glare shield gave better results in the low velocity region and Kevlar fared better in the high velocity regime. In 1999, Destefanis et al. [71], employed a wide-ranging light-gas gun for testing whipple shields for protecting the Columbus-module. Triple-walled shielding systems were subjected to over 100 hyper-velocity impact experiments. Two shield arrangements were used, one Aluminium based whipple shield and a transitional-bumper prepared of Kevlar™-epoxy and Nextel-fabric. Both these arrangements resulted in excellent performance in the ballistic-limits of 3 to 7 km/s with oblique angles ranging from 0 to 60°. The shield performance showed a non-monotonous variation with the increase in the impact velocities. It is also observed that with rise in impact angle ranging between 0 and 45°, the ballistic limit displayed a slight oscillation attributed to the level of disintegration of projectiles. In 1999, Destefanis [16] built the whipple shield with aluminium facets and intermediate layers, composed of Kevlar and Nextel. The tests were

conducted at a hypervelocity speed of 7 km/s with aluminium balls weighing 6.1 g. The presence of the intermediate layers enable a better impact resistance for these whipple shields. In the same year, Silvestrov et al. [72] tested ceramic/aluminium composites as at hypervelocities of 5.5 to 7.5 km/s. However, the performance of ceramics were inferior to that of convetional whipple shields. Lamontage et al. [73] analyzed the response of carbon fibre/PEEK composites subjected to hypervelocity impact using a light gas gun, shooting aluminium shells of diameters 1 mm and 2 mm at a velocity of 5 km/s. The oblique impact angles used were 0°, 30° and 45°. The researchers observed the lack in the cone symmetry about the projectile velocity vector. In 1999, Nebolsine et al. [74] studied the phenomena of rod-erosion for various hypervelocity-impact conditions and for different materials available in the Naval Research Laboratory database (J.J. Condon et al. [75, 76], and the works of Baker et al. [77]). The range of the hypervelocities were varied between 2.6 to 6.1 km/s. A semi-empirical equation was developed for normalizing the rod-erosion data based on the results from 157 tests. In year 1999, Orphal [78] studied the behaviour of residual projectile fragments obtained during the impact of steel spheres at 4.57 km/s onto laminated target whipple shields. Highly oblique impact angles ~ 60° to 80° were employed for the impact studies. Flash X-rays were employed for the fragment characterization. In 1999, Taylor et al. [79] studied the response of a whipple shield comprising two layers- a 1.6 mm thick carbon fibre reinforced plastic facing with a 45 mm aluminium honeycomb. The performance was compared to a Cour-Palais Whipple bumper shield. It was observed that the wall thickness played a negligible role in arresting the impact [80]). An empirical relation between the damage endured by the honeycomb structure and the impact energy was determined. The equation was validated with the ballistic limit curve of the used conventional Whipple bumper. In 2000, Piekutowski et al. [81] conducted a number of depth-of-penetration experiments with 6061-T6 aluminium sheets as the target. Point-nosed projectiles of diameter 7.11 mm and length 71.12 mm (made from 4340 steel and AerMet 100 steel) were chosen for the hypervelocity impact experiments at launching velocities of 0.5 to 3 km/s using a powder gun. Depth of penetration data and cavity expansion data were compated to analyze the performance. In 2001, Palmieri et al. [82], performed light-gas gun tests to validate the hydro-code simulation output conducted on gas filled pressure-vessel shields. The impact tests were carried out such that back-wall plate penetration was caused without perforation or leakage. In 2001, Vlasov et al. [83] extended the Whipple shield principle to shaped charge jets. A test was conducted which consisted of multi-spaced metal shields (0.2 to 0.5 mm thick). It was observed that the differential mass efficiency of the said systems was better than steel by a factor of 5 to 7, providing a means to make the whipple shields lighter. In 2006, Ohtani et al. [84] carried out hyper velocity impact experiments on cryogenically cooled aluminium alloys at 122K. Aluminium spheres at 1.95 km/s velocity were impinged against the target material comprising 2 mm AA5052-H34, 5 mm thick AA2024-T3 aluminium shields and 3.3 mm thick Kevlar fiber reinforced polymer plate. AA2017-T4 projectile of diameter 7.9 mm was used for causing the impact. The hypervelocity impact were carried out inside a cryogenic chamber cooled by liquid nitrogen. The debris cloud visulailzation was done by shadowgraph employing a high-speed digital video camera. Low orbit flights are marred with the presence of space debris and meteoroids which physically impact the spacecraft at hypervelocities causing catastrophic failures. In 2008, Gongshun et al. [85] made use of a two-stage light gas gun which launched aluminium alloy (with T4 temper) sphere projectiles at a hyper-velocity range of 0.69 km/s to 6.98 km/s on aluminium whipple shields. The crater distribution on the rear wall was studied. The craters were formed with a hemispherical geometry with the area increasing with increase in impact velocity and projectile diameter. In 2011, Ryan et al. [47], studied the shattered regime of the whipple shield. Numerous HVI experiments were executed for constant diameters of projectile, thickness of the bumper, and space between the shield, whereas thickness of rear wall was increased in order to regulate the failure boundaries. Subsequently, a rapid rise in the shielding function was observed for velocities between 3.1 and 4.0 km/s when compared to the expected ballistic limit equation. Constant performance was noted for velocities between 4.0 and 5.0 km/s. For velocities between 5.0 and 6.0 km/s, the perforation of the shields were extensive. In 2011, Piekutowski et al. [86], conducted a series of 18 impact experiments on whipple shields and compared the response with the estimated ballistic-limits in the higher regime of the hypervelocity limits. Under these conditions, the kinetic energy of the particles is tremendous enough to melt and vaporise the material of the particles. BLEs established at NASA-JSC was utilised to regulate insignificant failure-thresholds for dual arrangements of all-aluminium whipple shields. Al2017 (T4) spherical models were used to test the shield by varying the velocities and diameters between 6.94 to 9.89 km/s and 1.40 to 6.35 mm respectively. In this study, two types of Al-alloy rear-walls were used. The whipple shields displayed better resilience to the increase in the impact velocities. In 2011, Ryan et al. [87] conducted a series of 66 hypervelocity impact tests in studies comprising aluminium, titanium, stainless steel, copper, nickel, carbon fibre as the shielding materials in different whipple shield configurations. The configurations involved monolithic plates, open-cell foam and flexible fabrics, arranged in single, double and triple bumper arrangements. The experiments consisted of impacting the shield

with a debris cloud travelling at 6.8 km/s. The configuration with aluminium outer bumper and foam inner bumpers outperformed the other configurations. In 2011, Jiyun et al. [88] studied effects of the hypervelocity impact on whipple Shields at cryogenic temperature of −150° C. Liquid nitrogen was used to maintain cryogenic conditions. Hyper velocity impact were conducted using a two-stage light gas gun. The key metrics of bumper penetration,debris cloud,and rear wall damage were compared. In year 2012, Huang et al. [89] proposed a whipple shield structure reinforced with an amorphous alloy. The shields were subjected to hypervelocity impact tests at velocities of 3.5 and 5.5 km/s using a two-stage light-gas gun.The shield structure was able to cause fragmentation of the orbital debris and withstant the high shock pressures. In 2013, Song et al. [90], developed a momentum-diagnostic technique to govern the momentum distribution of a debris-cloud.The spatial distribution of the debris-cloud caused due to collision of bumper and projectile was evaluated. Two experimental methods comprising micro-fragments and planar impact were conducted to assess the rear-wall desecrating impact of a debris-cloud and the toughness of material during fragment penetration. At velocities between 4 and 6 km/s, it is seen that the fabric laminate disintegrates into finer fragments. In 2013 Khatiwada et al. [91] fabricated epoxy matrix composites with ultra-high molecular weight polyethylene nanoparticles and carbon nanotubes for the application of whipple shield bumper. The bumpers were tested for hypervelocity impact in the velocity range of 6.5 to 7 km/s. Although, the perforation characteristics of the bumper material was superior to that of aluminium bumpers, the efficiency was comparatively lower. In 2015, Miller et al. [92] experimentally studied the impact of steel and aluminium projectiles on double-walled whipple shields. The factors taken up for the study consisted of the thickness of the wall, the density and the impact speed. In 2015, Poniaev et al. [93], developed a lab-scale rail gun to bombard a fiber-metal laminate whipple shield comprising an external aluminium bumper followed by ultra-high molecular weight poly-ethylene core. It was observed that the factors such as area and degree of the perforation depended on the thickness of the aluminium bumper. In 2015, Hofmann et al. [94] compared stuffed Whipple shields (with metallic glass) and shields used in International space stations, the former showed a better performance under hypervelocity impact. Table 4 shows the setup used for different experimental studies of HVI on whipple shields.

In 2016, Moon et al. [104] proposed a hybrid composite shield (HCS) comprising a preliminary bumper, an ultra-thin intermediary fabric layer and a rear-plate. The critical specific energy of absorption was derived in this model along with the fabric pull-out through the penetrated hole of the rear-plate. Different types of hybrid composite shields were tested using a 2-stage light-gas gun. The gun was used to accelerate spherical aluminium projectiles of diameter 5.56 mm to 1 km/s. When weak materials like polyamide, polyethylene and PMMA were used for the rear-wall, the specific energy of absorption decreased. In 2016, Ke et al. [105] explored triple-layered stuffed whipple shields composed of ceramic and aramid fibers. A debris cloud of spherical aluminium was hurtled at the bumper at a speed of 6.2 km/s and the cracking mechanism of the shield was analyzed. Perfect bonding between the three layers resulted in better performance than thin air gaps. In 2016, Huang et al. [106] designed a hypervelocity impact shield, comprising a TiB_2 front bumper. The experiments were conducted at speeds of 3 km/s, 5 km/s and 7km/s. As compared to aluminium bumpers, TiB_2 based bumpers displayed better against the space debris, with enhanced performance at 5 km/s.

In 2016, Guan et al. [107] studied stuffed whipple shields along with aluminium whipple shields, with target application in on-orbit Cryogenic Propellant storage. The hypervelocity impact tests were conducted using a two-stage light gas gun, using Al spherical projectiles.

In 2016, Wen et al. [108] experimented with stuffed shields by considering wood which is a light weight, inexpensive and high yield strength material. The hypervelocity impact tests were done at speeds of 4.79 to 7.24 km/s. The results were compared with aluminium triple-walled and Kevlar fabric stuffed shields. It was concluded that the wood stuffed shield performs similar to that of Kevlar stuffed shields and outperforms triple-walled aluminium shields. In 2017, Mespoulet et al. [109], conducted hyper-velocity impact tests for millimetre(mm) sized orbital debris in the range 6 km/s to 15 km/s for single-plate and honeycomb configuration whipple shields. The mm-sized debris pose a potent risk to the structure of the space vehicles since they are hard to detect and track using radars. Explicit analytical tools like X-ray flash photography, high-speed camera were used for observing the phenomenon of ejecta-projection. Furthermore, the effect of ejecta-tunnelling for honeycomb configuration was emphasized.

Development of inflatable structures was a breakthrough in the space flight industry since it provides a flexibility to launch and install a large space setup in the outer orbits. To safeguard these structures, Kim et al. [110], developed shock shields comprising front bumper made of multi-layered ceramic fabrics and carbon fiber composites. The carbon fiber bumpers performed better than the ceramic fabric ones against hypervelocity impact. In 2019, Kim et al. [111] identified that Fish-scale armour also known as ”Dragon skin” was effective for flexible bumper structures. In 2018, Fa-wei et al. [112], used aluminium honeycomb and aluminium mesh supporting a basalt fabric. The thickness of the rear-plate and the front bumper were kept as 1 mm while the stuffed layer was located 100 mm from the front bumper. The target was impacted by a 5 mm diameter aluminium

Table 4 Details and specifications of the hypervelocity-impact experimental setup

Researchers	Facility	Impact velocity (km/s)	Test equipment	Target material	Key observations
Liu [22, 95]	State Key Laboratory of Explosion Science and Technology, China	2.511	Two-stage light gas gun	Al plate (1 mm thick)	No penetration
Ryan [28]	NASA-JSC	3	Two-stage light gas gun	AA6061-T6	AA2017-T4 projectile, Perforation observed
Ji-Hun Cha [96]	KAIST	3.269	Ultra high molecular weight polyethylene	Two-stage lightweight gas gun	Max. perforation at high temperature
Poniaev [97]	Ioffe Institute	3.96	Compact rail gun with plasma piston	Aluminium and UHMWPE	Polycarbonate cube projectiles with 2-mm ribs, Destruction of the impactor and aluminium plate
Olivieri [98]	CISAS Hypervelocity Impact Facility	4.7	Two-stage light gas gun	3D printed shields	Al-1100 spherical projectiles, No perforation
Wen [99]	CARDC	4.86	Hypervelocity range	Pinewood, Aluminium, Nextel/Kevlar	AA2024 projectiles (5-8 mm diameter), Stuffed shields showed low perforation
Jing [100]	CARDC	4.9	Hypervelocity range	Aerogel/ Fiber-glass composite	Aluminium projectiles (4-6 mm diameter)No obvious damage was found on the rear wall
Fa-wei [101]	CARDC	5.01	HVI Range	Basalt, aramid and Aluminium honeycomb	Al projectile (5 mm diameter), Severe perforation of rear wall
Huang [89]	CARDC	3.5-5.5	Two-stage light gas gun	Fe-based amorphous alloy with LY12 aluminium substrate	Craters and spallation observed, Partial or nil perforation on Rear wall
Piekutowski [48]	NASA-JSC	> 9	Two-stage light gas gun	Aluminium	AA2017-T4 spherical projectiles, Central spall with several open cracks at edges
Wen [49]	CARDC	8.31	Two-stage light gas gun	2A12 aluminium	Impact classified as intact, ruptured, and smashed, Al2017-T4 spherical projectile 6.35 diameter
Song [102]	IFP of China Academy of Engineering Physics	9	Electric gun	Carbon-fiber reinforced polymer	Mylar flyer plate 0.1 mm thick, Perforation crater depth and hole diameter compared
Liu [52]	China Academy of Space Technology (CAST)	2.9-5.5	2 J pulsed LDF setup	Polyimide material with three thicknesses (8, 12.5, 25 μm)	Perforation damage in the impact zone, radial cracks studied
Wells [103]	Space Research Institute Auburn	5-12	Plasma drag gun	Coated thermoplastic	Impact at cryogenic (40 K) temperature produced shear damage and elevated temperature (420 K) showed bulge damage, 0.01-0.1 mm sodalime spherical projectiles

projectile for velocities between 4 and 5 km/s. The honeycomb led to weight reduction of the shield and was also able to tolerate the impact from the enormous kinetic energy of the debris cloud. In 2018, Voillat et al. [12] carried out experiments on A357 aluminium stochastic foams bombarded with spherical aluminium projectiles 2 mm in diameter accelerated to velocities of 6.7 to 7.0 km/s. The angle of impact was varied to study the response of the foams. Between 0 and 12°, failure of the structure was observed. For higher angles, the structure was capable of withstanding the impact. In 2018, Nam et al. [113] designed and fabricated a space shield system (using aramid and epoxy composite) fitted with an electromagentic-wave absorption system for stealth. The hyper-velocity impact tests of this shield were done using a two-stage gas gun shooting projectiles at velocities in the range of 2.7 to 3.2 km/s. The failures observed in the silver coated composite and the uncoated composite were similar. Inter-laminar shear-strength tests were also conducted for the proposed shield system to confirm its usability and application in military space programs.

In 2019, Liu et al. [114] conducted an analysis on shock acoustic Emission (AE) waves formed due to hypervelocity impact on dual-layered Whipple shielding arrangement. The effects of the projectiles at numerous impact velocities on the structural shielding with different thicknesses were observed. The localisation in the hypervelocity impact was studied using a progressive process signalling and enhanced delay-sum approach for the transmitted acoustic emission wave. The acoustic sensors were made of lead zirconium tartrate which was used for the detection of the acoustic emission. In 2019, Wen et al. [115], studied three different shielding systems- fiberglass/ aerogel composite attached to aluminium rear wall, wood/ polyurethane plate attached to aluminium rear-wall and all-aluminium whipple shield. Aluminium spheres of 5 mm diameter accelerated to velocities between 4.62 and 4.90 km/s were used to achieve the hypervelocity impact on the shielding systems. In 2019, Cao et al. [116] identified that the hypervelocity impact generates a debris cloud that can lead to numerous craters and cracks on the rear wall. These cracks can ultimately lead to the failure of the shielding system. The material degradation studies were conducted using optical microscopy, laser scanning microscopy and X-ray diffraction. After the tests, two types of damages were identified i.e. micro-voids and micro-cracks which were found beneath the pitting damage area. When subjected to high hypervelocity impacts, which create high compressive strains, the micro-voids further expand at the grain boundaries. As an upgradation in Whipple shields for spacecraft structures to have better shielding from orbital debris, Ti-Al nylon (impedance graded materials) enhanced shields were proposed by Zhang et al. [117]. The Ti-Al nylon shields displayed better characteristics during hypervelocity impacts as it can generate higher shock pressures conducive for a better fragmentation process of the orbital debris. In 2019, Zhang et al., [118] studied Al/Mg impedance graded material and monolithic aluminium shields. The test comprised of a hypervelocity impact test using a light-gas gun, shooting projectiles at velocities of 3.5 to 6.5 km/s. This experiment showed that the Al/Mg bumper was superior to the conventional Al one despite the fact that the magnitude of the shock pressures generated in the two shields was similar. A ballistic limit curve for the Al/Mg Whipple shield was developed.

In 2020, Cha et al., [119] studied a WS configuration consisting of ultra-high molecular weight poly-ethylene in order to enhance the competence of the shield against the orbital debris over traditional whipple shields. Ballistic-limit was examined using a two staged light-weight gas-gun at velocity about 4 km/s which was used to accelerate aluminium projectiles of 5.56 mm diameter. The results stated that ultra-high molecular weight polyethylene showed superior ballistic performance compared to the traditional whipple shields. Additionally, it could be used for protection against cosmic-radiation. In 2020, Xuezhong et al. [120] conducted hyper-velocity impact experiments and numerical-simulations in order to examine the capability and functioning of shielding systems comprising of a separated rear-wall. Two kinds of spherical Al-projectiles were considered with diameters 6 mm and 4 mm at velocities of 4.7 to 8.3 km/s respectively. The whipple shield and a separated rear-wall shielding system of similar areal density were used as the targets. The performance of the rear-wall shielding system was enhanced compared to the conventional whipple shields. The detached surface of the separated rear-wall shielding system attenuates the dissemination of the wave caused by the energy of impact. The decrease in the free-surface velocities on the back end of the rear-wall resulted in lower rear-wall surface damage. For an in-orbit spacecraft the biggest factor that questions its survivability is the spacecraft's capacity to sustain damage from the hypervelocity space debris. In 2020, the authors Huang et al. [11] conducted an experiment to test the bumper Whipple shield fabric made of B_4C/Al composite which is lightweight and is manufactured by the pressure-less pre-sintering and Al infiltration under vacuum. The experiment was conducted at speed of 3Km/s to 6.5Km/s. This experiment is conducted so as to get a theoretical background on the materials for proper design of the required configuration. The results obtained pointed towards the conclusion that the B4C/Al bumper showed a 20% better performance than the conventional Al-alloy Whipple shield.

3D printing has emerged as a novel manufacturing technique for parts that are tough or expensive to fabricate. Complex and intricate shapes with geometry suiting novel celled structures could be easily printed using suitable materials. In 2020, Olivieri et al. [121] created a framework of 3D printed shields which were meant to protect micro-satellites. These

were subjected to hypervelocity impact from millimetre-sized debris. It was concluded that the 3D printed shields have better capacity to fragment impacting projectiles as compared to equivalent honeycomb cored shields.

With deteriorating space environment due to space debris, of late, impact induced energetic composites are being used. In 2020, Ren et al [122] studied the impact induced reaction aspects of poly tetra fluoro ethylene (PTFE)/Al and PTFE/Ti whipple shields. The experiment consisted of hurtling projectiles using a two-stage light gas gun at the two whipple shields and the results were compared to that of a Al2024 bumper. The reactive materials displayed better defensive capabilities against hypervelocity impact. It was also concluded that PTFE/Al was more efficient than PTFE/Ti. Large stand-off between the front bumper and the rear wall are constrained by certain space applications. In 2020, Poole et al. [123] introduced the PrintCast technique to fabricate monolithic strucutres. These materials were also tested under hypervelocity impact conditions to get an in-depth information about the failure characteristics of the said materials.

Results and Discussions

The past 20 years of research have narrowed down the requirements for ideal whipple shields. The effectivness of the whipple shields are defined by the ability of the material to withstand hypervelocity impact between 2 and 18 km/s, for various shapes, sizes and materials of the projectiles (Refer Table 5), the angles made by the velocity vectors relative to the whipple shield face, the ability to attenuate shock waves generated on impact and piercing effects of the debris cloud occuring due to fragmentation.The experimental and numerical methods have been extensively used for comparing different materials with conventional aluminium shields (Fig. 7).

The experiments carried out are limited to a scaled down, imitative environment. The advanced numerical techniques were able to scale the gaps between the current experimental setup and actual operational conditions [32]. The simulation tools like SPH, CTH, AUTODYN-2D, PAMSHOCK and Eulerian adaptive-mesh hydrodynamics were popularly used for the past three decades in assessing the performance of whipple shields.

For accurate simulation of the proposed whipple shields, a representative debris cloud and its interaction with the whipple shields determines the effectiveness of the shielding systems. The cloud comprising orbital debris and micrometeoroids were simulated by a stream of projectiles of spherical or ellipsoidal shapes made up of materials such as aluminium, aluminium alloys, polyethylene, cadmium, steel, and lead. Although the hyperimpact velocity is the primary parameter for testing the effectiveness of the shield, there are several secondary parameters like critical particle diameter, particle shape, particle material, mass threshold, and momentum, influencing the shield performance (Table 6).

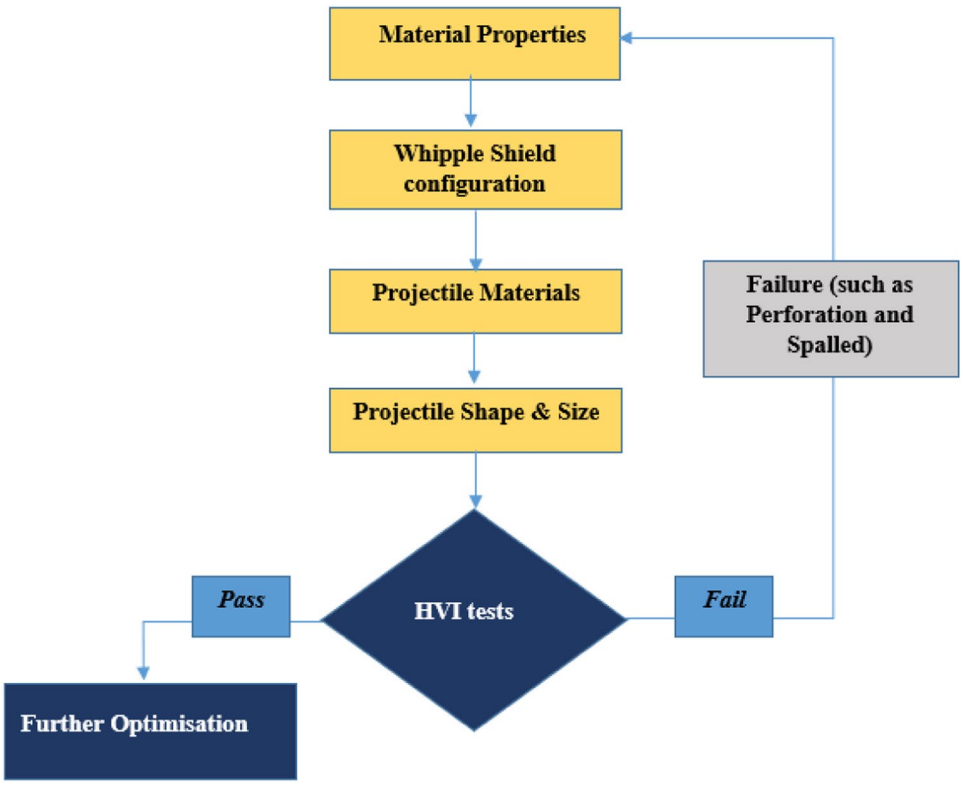

Fig. 7 Selection of whipple shield configuration and material properties

Table 5 An overview of projectile shape, size and whipple shield materials

Author	Projectile shape	Projectile diameter (mm)	Target shield material	Diagnostic equipment
Christiansen et al. [26]	Spherical (Al)	3.2	MDM and MS	High speed digital photography
Katayama et al. [23, 24]	Spherical(PE)	14.2	AA2024-T3	X-ray CT scanning
Kerr et al. [53]	Spherical	10.01	Al-double bumper (AA6061-T6 and AA2024-T3)	High speed camera
Cour palais et al. [41]	Spherical (Cd)	6.55	Al	X-radiography and High speed camera
Rabb et al. [40]	Spherical (Al)	6	Al	Debris Cloud profiling
Taylor et al. [44]	Spherical(Al)	4.4	Al	Flash X-ray stations
Palmieri et al. [43]	Spherical(Al)	5.5	AA2024-T3	X-ray stations
Hiermaier et al. [33]	Ellipsoid (Al alloy)	5	Al alloy	Graphical damage profiling
Zhang et al. [61]	Spherical	7.9	Al-Bumper and Egg box panel	Critical penetration and impulse
Moon et al. [104]	Spherical (AA2017-T4)	5.56	Carbon fibre reinforced polymer (CFRP)	Chronographs for velocity measurement
Kim et al. [111]	Spherical (AA2024-T4)	5.56	AA2017-T4, AA6061 T6, SUS304	High speed camera
Wen et al. [120]	Spherical (AA2024)	6	AA6061	Laser shadowgraphy
Huang et al. [11]	Spherical (AA2024)	5	B_4C/Al composite	Laser Shadowgraph Imager
Silvestrov et al. [72]	Spherical (steel)	0.9 and 0.83	Disperse ceramic inclusions of SiO_2 / $A1_2O_3$	Analog camera
Huang et al. [89]	Spherical (LY-12 Al)	4	LY-12 Al	Scanning electron microscopy of perforated surface
Zhang et al. [118]	Spherical (Al)	3.25,4.5,4.75	Al/Mg, 2A12, AZ31B	Laser shadowgraph imager
Hofmann et al. [124]	Spherical (Al)	3.17	Ti-based Bulk metallic glasses, LY12 Al	High speed camera
Vlasov et al. [83]	Spherical (Pb)	7.6	Pb	
Ren [122]	Spherical (AA2024)	6	PTFE/Al, PTFE/Ti and AA2024	High frequency photography
Wen et al. [49]	Spherical (AA 2017-T4)	7-14	A1	Flash X-ray imaging
Huang [106]	Spherical (LY12-Al)	3	TiB_2-based composite, AA6061	Laser shadowgraph imager
Kim et al. [110]	Spherical (AA2014-T4)	5.56	AA6061 T6, Carbon fabric, Twaron fabric, zylon fabric	ImageJ software with HP scanjet
Wells [103]	Spherical (Soda lime glass)	0.04-0.1	Kapton film with vapor deposited aluminium on both sides (Cryogenic 40 K)	Streak camera and photomultiplier tube
Ohtani et al. [84]	Spherical (Al)	15-51	Cryogenically cooled Aluminium (122K)	High speed camera and ruby laser Shadowgraphy
Kumar et al. [125] [125]	Spherical (AA2017-T4)	5.56	Polybenzimidazole coated carbon fiber composite	Laser intervalometer
Numata et al. [126]	Spherical (Al)	7.94	AA5052-H34 (120-293 K)	Helium-Neon laser shadowgraph Imager, High Speed Camera

The diameters of the projectiles were found to vary from 3 to 14 mm. The era of whipple shield materials began with aluminium and its alloys (AA2017, LY12, AA 2024). Upon hypervelocity impact of a projectile onto a bumper, a complex process of dynamic fracture and deformation may occur. As a result, the projectile and bumper can fragment, melt, liquidize or vaporize. Thus, the purpose of bumper in hypervelocity impact shielding system becomes vital. There were novel materials like Ti-Al-nylon, carbon fiber, Kevlar-Nextel, Glare, Dragon-skin, UHMWPE which were used as hybrid arrangements in front bumpers of the whipple shields. The configurations were modified to stuffed whipple shields with honeycomb and celled cores to absorb the shock energy. Attempts were also made to vary the areal density

Table 6 Overview of HVI database with the data sources

Source	Total no. of tests			Perforation/spalled	Passed
	Experimental	simulation	Total		
Christiansen [127]	9	–	9	6	3
Schonberg [128]	228	–	228	157	71
Christiansen [26]	55	–	55	19	36
Kerr [53]	–	21	21	12	9
Rabb [40]	–	20	20	11	9
Destefanis [71]	28	–	28	10	18
Palmieri [82]	–	26	26	17	9
Kerr [42]	3	14	17	11	6
Gongshun [85]	63	–	63	43	20
Piekutowski [86]	18	–	18	8	10
Ryan [47]	82	–	82	40	42
Ryan [87]	66	–	66	31	35
Ryan [129]	9	–	9	6	3

of the whipple shields for better dissipation of the kinetic energy of the debris cloud.

Limitations and Future Scope

The early 90s faced the limitation of accurate and effective experimental capability. Only a limited amount of data could be gathered due to the inferior technology. For instance, Miller et al. [92], developed a double-walled Whipple shield to study the effects of three factors, namely, the thickness of the wall, the density and the impact speed. The statistics were mainly focussed on the aluminium alloy rear wall and the data was restricted to not include the fragmentation characteristics. Likewise, Putzar et al. [67], proposed a conservative ballistic limit equation, with no data points for penetration beyond the ballistic limit curve. Especially at low impact angles and low impact speeds, the proposed BLE was observed to be overly conservative. Similar effects have been observed in the cases of the ESA Columbus debris shield and the NASA SW shield. The fragmentation characteristics could be studied through advanced high speed photography and image capturing tools in the shatter regime of the whipple shields.

Designs of inflatable structures and their excellent response to hypervelocity impact are slowly gaining popularity. Launching such flexible and versatile structures promises to reduce costs and expand the areas of application. The concept of a multi-shock shield with flexible materials was introduced to meet the specific demand of having a spacious space structure. It is believed that the multi-shock shield concept was also used in the Bigelow Expandable Activity Module, BEAM which was the first inflatable activity module in space. Though a higher number of bumpers and greater stand-off distance can certainly improve the performance, the increments would be less effective, unless geometry is appropriately designed taking into consideration the target and impact conditions. Metallic glass as a stuffing material shows promise due to its high hardness, low melting point, low density and ability to form corrugated structures. Auxetic (negative Poisson's ratio) materials are gathering a phenomenal interest from shielding perspective which can be employed for the honey-comb core of whipple shields. This can impart significant impact resistance against the space debris [130].

Conclusion

The review briefly covers the advances in Whipple shield and its components. The promising materials, novel configurations with stuffed shields, inflatable structures span the physical requirement of whipple shields. The experimental and numerical techniques employed reveal the operational features of whipple shields. Although the investigations cover different sizes, shapes and materials of the projectiles, nevertheless, in a debris cloud, the standard deviation of the shape, size as well as the type of material may be significant to account for, which needs to be addressed in future research. Only then can an effective model may be developed for predicting the life of whipple shields used on space vehicles. With the ever-populating outer space, the probability of impact of debris cloud with satellites and space vehicles would only rise in future necessitating tougher, stronger, reliable and resilient materials for whipple shields with the fabrication of complex shapes and geomtry made possible by the rapid prototyping techniques like 3D printing, Stereolithography, Laser sintering.

Acknowledgements The authors would like to thank Dr. T G Pai, Professor, Department of Aeronautical and Automobile Engineering, MIT Manipal for his valuable suggestions.

Funding Open access funding provided by Manipal Academy of Higher Education, Manipal.

References

1. Gehring JW, Maiden CJ, McMillan AR, Sennett RE (1965) Experimental investigations of simulated meteoroid damage to various spacecraft structures, Summary report prepared for NASA, Houston, Texas
2. Christiansen EL (1990) Advanced meteoroid and debris shielding concepts. In: Orbital debris conference: technical issues and future directions 1990. https://doi.org/10.2514/6.1990-1336
3. Chhabildas LC, Hertel ES, Hill SA (1993) Hypervelocity impact tests and simulations of single whipple bumper shield concepts at 10km/s. Int J Impact Eng 14(1–4):133. https://doi.org/10.1016/0734-743X(93)90015-Y
4. Christiansen EL (1993) Design and performance equations for advanced meteoroid and debris shields. Int J Impact Eng 14(1–4):145. https://doi.org/10.1016/0734-743X(93)90016-Z
5. Lemmens S, Letizia F (2019) ESA annual space environment report. ESA Space Debris Office, Darmstadt, Germany, Tech. Rep. GEN-DB-LOG-00271-OPS-SD
6. Sunda S, Sridharan R, Vyas B, Khekale P, Parikh K, Ganeshan A, Sudhir C, Satish S, Bagiya MS (2015) Satellite-based augmentation systems: a novel and cost-effective tool for ionospheric and space weather studies. Space Weather 13(1):6
7. Carrasquilla MJ, Miller JE (2017) Shape effect analysis of aluminum projectile impact on whipple shields. Procedia Eng 204:308. https://doi.org/10.1016/j.proeng.2017.09.751
8. Khatiwada S, Armada CA, Barrera EV (2013) Hypervelocity impact experiments on epoxy/ultra-high molecular weight polyethylene fiber composites reinforced with single-walled carbon nanotubes. Procedia Eng 58:4. https://doi.org/10.1016/j.proeng.2013.05.003
9. Christiansen E(1990) Advanced meteoroid and debris shielding concepts. In: Orbital debris conference: technical issues and future directions, p 1336
10. Cherniaev A, Telichev I (2018) Sacrificial bumpers with high-impedance ceramic coating for orbital debris shielding: a preliminary experimental and numerical study. Int J Impact Eng 119(April):45. https://doi.org/10.1016/j.ijimpeng.2018.05.004
11. Huang X, Yin C, Ru H, Zhao S, Deng Y, Guo Y, Liu S (2020) Hypervelocity impact damage behavior of B4C/Al composite for MMOD shielding application. Mater Design 186:108323
12. Voillat R, Gallien F, Mortensen A, Gass V (2018) Hypervelocity impact testing on stochastic and structured open porosity cast Al-Si cellular structures for space applications. Int J Impact Eng 120(April):126. https://doi.org/10.1016/j.ijimpeng.2018.05.002
13. Mondolfo L (1971) Structure of the aluminium: magnesium: zinc alloys. Metall Rev 16(1):95
14. Zhao S, Song Z, Espinosa HD (2020) Modelling and Analyses of Fiber Fabric and Fabric-Reinforced Polymers under Hypervelocity Impact Using Smooth Particle Hydrodynamics. Int J Impact Eng 144(May):103586. https://doi.org/10.1016/j.ijimpeng.2020.103586
15. Huang X, Yin C, Ru H, Zhao S, Deng Y, Guo Y, Liu S (2020) Hypervelocity impact damage behavior of B4C/Al composite for MMOD shielding application. Mater Des 186:108323. https://doi.org/10.1016/j.matdes.2019.108323
16. Destefanis R, Faraud M, Trucchi M (1999) Columbus debris shielding experiments and ballistic limit curves. Int J Impact Eng 23:181. https://doi.org/10.1016/s0734-743x(99)00071-8
17. Hayhurst CJ, Livingstone IH, Clegg RA, Fairlie GE, Hiermaier SJ, Institut F, Str E, Lambert M, Noordwijk AZ(1998) Numerical simulation of hypervelocity impacts on aluminum and Nextel/Kevlar whipple shields. Proceedings of the Hypervelocity shielding workshop, 8 March, pp. 61–72
18. Ryan S, Kandanaarachchi S, Smith-Miles K (2015) Support vector machines for characterising whipple shield performance. Procedia Eng 103:522. https://doi.org/10.1016/j.proeng.2015.04.068
19. Ryan S, Thaler S, Kandanaarachchi S (2016) Machine learning methods for predicting the outcome of hypervelocity impact events. Expert Syst Appl 45:23. https://doi.org/10.1016/j.eswa.2015.09.038
20. Groenenboom PH (1997) Numerical simulation of 2D and 3D hypervelocity impact using the SPH option in PAM-SHOCK™. Int J Impact Eng 20(1–5):309. https://doi.org/10.1016/s0734-743x(97)87503-3
21. Buyuk M, Kurtaran H, Marzougui D, Kan CD (2008) Automated design of threats and shields under hypervelocity impacts by using successive optimization methodology. Int J Impact Eng 35(12):1449
22. Liu M, Liu G (2010) Smoothed particle hydrodynamics (SPH): an overview and recent developments. Arch Comput Methods Eng 17(1):25
23. Katayama M, Toda S, Kibe S (1997) Numerical simulation of space debris impacts on the whipple shield. Acta Astronaut 40(12):859. https://doi.org/10.1016/S0094-5765(97)00128-8
24. Katayama M, Kibe S, Toda S (1995) A numerical simulation method and its validation for debris impact against the whipple bumper shield. Int J Impact Eng 17(4–6):465–476
25. Wei Ke F, Huang J, Zhong Wen X, Xia Ma Z, Liu S (2016) Test study on the performance of shielding configuration with stuffed layer under hypervelocity impact. Acta Astronaut 127:553. https://doi.org/10.1016/j.actaastro.2016.06.037
26. Christiansen EL (1993) Design and performance equations for advanced meteoroid and debris shields. Int J Impact Eng 14(1–4):145
27. Cour-Palais B, Piekutowski A, Dahl K, Poormon K (1993) Analysis of the UDRI tests on Nextel multi-shock shields. Int J Impact Eng 14(1–4):193
28. Ryan S, Bjorkman M, Christiansen EL (2011) Whipple shield performance in the shatter regime. Int J Impact Eng 38(6):504. https://doi.org/10.1016/j.ijimpeng.2010.10.022
29. Ryan S, Christiansen EL (2011) A ballistic limit analysis programme for shielding against micrometeoroids and orbital debris. Acta Astronaut 69(5–6):245. https://doi.org/10.1016/j.actaastro.2011.04.012
30. Ryan S, Thaler S (2013) Artificial neural networks for characterising Whipple shield performance. Int J Impact Eng 56:61. https://doi.org/10.1016/j.ijimpeng.2012.10.011
31. Ryan S, Kandanaarachchi S, Smith-Miles K (2015) Support vector machines for characterising Whipple shield performance. Procedia Eng 103:522
32. Hayhurst CJ, Livingstone IH, Clegg RA, Fairlie GE, Hiermaier SJ, Lambert M (1998) Numerical simulation of hypervelocity impacts on aluminum and Nextel/Kevlar Whipple shields. In: Proceedings of the hypervelocity shielding workshop, p 61
33. Hiermaier SJ, Schäfer FK (2003) Simulation of ellipsoidal projectile impact on whipple shields. Int J Impact Eng 29(1–10):333
34. Silnikov M, Guk I, Nechunaev A, Smirnov N (2018) Numerical simulation of hypervelocity impact problem for spacecraft shielding elements. Acta Astronaut 150:56

35. Groenenboom PH (1997) Numerical simulation of 2D and 3D hypervelocity impact using the SPH option in PAM-SHOCK^{TM}. Int J Impact Eng 20(1–5):309
36. Chhabildas L, Hertel E, Hill S (1993) Hypervelocity impact tests and simulations of single whipple bumper shield concepts at 10 km/s. Int J Impact Eng 14(1–4):133
37. Alme ML, Rhoades CE Jr (1995) A computational study of projectile melt in impact with typical whipple shields. Int J Impact Eng 17(1–3):1
38. Hultgren R, Desai PD, Hawkins DT, Gleiser M, Kelley KK (1973) Selected values of the thermodynamic properties of the elements. National Standard Reference Data System
39. Fahrenthold E (1995) Oblique hypervelocity impact simulation for Whipple shield-protected structures. Int J Impact Eng 17(1–3):291
40. Rabb RJ, Fahrenthold EP (1999) Numerical simulation of oblique impact on orbital debris shielding. Int J Impact Eng 23(1):735
41. Cour-Palais B, Littlefield D, Piekutowski A (1995) Using dense, low melting point projectiles to simulate hypervelocity impacts on typical spacecraft shields. Int J Impact Eng 17(1–3):241
42. Kerr J, Christiansen E, Crews J (1996) AIP conference proceedings. American Institute of Physics, vol 370, p 1167
43. Palmieri D, Faraud M, Destefanis R, Marchetti M (2001) Whipple shield ballistic limit at impact velocities higher than 7 km/s. Int J Impact Eng 26(1–10):579
44. Taylor EA (2001) Simulation of hollow shaped charge jet impacts onto aluminium whipple bumpers at 11 km/s. Int J Impact Eng 26(1–10):773
45. Williamsen J, Evans S (2017) Orbital debris momentum transfer in satellite shields following hypervelocity impact, and its application to environment validation. Procedia Eng 204:500
46. Zhang X, Jia G, Huang H (2014) An approach for constituting double/multi wall BLE by single wall BLE of spacecraft shield. Int J Impact Eng 69:114. https://doi.org/10.1016/j.ijimpeng.2014.02.009
47. Ryan S, Bjorkman M, Christiansen E (2011) Whipple shield performance in the shatter regime. Int J Impact Eng 38(6):504
48. Piekutowski AJ, Poormon KL, Christiansen EL, Davis BA (2011) Performance of whipple shields at impact velocities above 9 km/s. Int J Impact Eng 38(6):495. https://doi.org/10.1016/j.ijimpeng.2010.10.021
49. Wen K, Chen XW, Chi RQ, Lu YG (2020) Analysis on the fragmentation pattern of sphere hypervelocity impacting on thin plate. Int J Impact Eng 146(September):103721. https://doi.org/10.1016/j.ijimpeng.2020.103721
50. Horner J (2008) A comparison of ballistic limit with adaptive-mesh Eulerian hydrocode predictions of one-and two-plate aluminum shielding protection against millimeter-sized Fe-Ni space debris. Int J Impact Eng 35(12):1602
51. Tjønn E (2017), Modeling and simulation of hypervelocity impact against debris shields for spacecraft protection. Master's thesis, NTNU
52. Liu T, Zeng Z, Zhang X, Qiu X, Cheng Z, Wang L, Jia S, Cai J (2019) Performance of polyimide film under hypervelocity impact of micro flyer: experiments and simulations. Acta Astronaut 159:452
53. Kerr JH, Fahrenthold EP (1997) Three dimensional hypervelocity impact simulation for orbital debris shield design. Int J Impact Eng 20(6–10):479
54. Hopkins A, Lee T, Swift H (1972) Material phase transformation effects upon performance of spaced bumper systems. J Spacecraft Rockets 9(5):342
55. Heuzé O (2012) General form of the Mie-Grüneisen equation of state. CR Mec 340(10):679
56. Schonberg WP, Compton L (2008) Application of the NASA/JSC Whipple shield ballistic limit equations to dual-wall targets under hypervelocity impact. Int J Impact Eng 35(12):1792
57. Bohannan A, Fahrenthold E (2009) Simulation of STF Kevlar shielding performance in a stuffed whipple configuration. In 50th AIAA/ASME/ASCE/AHS/ASC Structures, Structural Dynamics, and Materials Conference
58. Hussain G, Hameed A, Barton P, Malik A (2011) Effectiveness of whipple shields with backplate compared to homogeneous mild steel alone against EFP threats. Proceedings of the 26th international symposium on ballistics
59. Hussain G, Hameed A, Horsfall I, Barton P, Malik A (2012) Experimental and simulation optimization analysis of the Whipple shields against shaped charge. Acta Mech Sin 28(3):877
60. Ryan S, Thaler S (2013) Artificial neural networks for characterising Whipple shield performance. Int J Impact Eng 56:61
61. Xt Zhang, Jia Gh, Huang H (2014) A fast numerical approach for Whipple shield ballistic limit analysis. Acta Astronaut 93:112
62. Zhang X, Liu T, Li X, Jia G (2016) Hypervelocity impact performance of aluminum egg-box panel enhanced Whipple shield. Acta Astronaut 119:48
63. Carrasquilla MJ, Miller JE (2017) Shape effect analysis of aluminum projectile impact on whipple shields. Procedia Eng 204:308
64. Jing L, Lin J, Xuezhong W, Jie H, Qing L, Xuegang H, Sen L (2017) Primary study on shielding performance of aerogel/fiberglass composite stuffed in thermal insulation shield. Procedia Eng 204:429
65. Deconinck P, Abdulhamid H, Héreil P, Mespoulet J, Puillet C (2017) Experimental and numerical study of submillimeter-sized hypervelocity impacts on honeycomb sandwich structures. Procedia Eng 204:452
66. Pydah A, Batra R (2018) Blast loading of bumper shielded hybrid two-core Miura-ori/honeycomb core sandwich plates. Thin-Walled Struct 129:45
67. Putzar R, Zheng S, An J, Hovland S (2019) A stuffed Whipple shield for the Chinese space station. Int J Impact Eng 132:103304
68. Cour-Palais B (1969) Meteoroid protection by multiwall structures. In Hypervelocity Impact Conference, vol 1969, p 372
69. Morrison RH (1970) Simulation of meteoroid-velocity impact by use of dense projectiles. National Aeronautics and Space Administration
70. Lambert M, Schneider E (1997) Hypervelocity impacts on gas filled pressure vessels. Int J Impact Eng 20(6):491. https://doi.org/10.1016/S0734-743X(97)87437-4
71. Destefanis R, Faraud M, Trucchi M (1999) Columbus debris shielding experiments and ballistic limit curves. Int J Impact Eng 23(1):181
72. Silvestrov VV, Plastinin AV, Pai VV, Yakovlev IV (1999) An investigation of ceramic/aluminium composites as shields for hypervelocity impacts. Int J Impact Eng 23:859. https://doi.org/10.1016/s0734-743x(99)00130-x
73. Lamontage CG, Manuelpillai GN, Taylor EA, Tennyson RC (1999) Normal and oblique hypervelocity impacts on carbon fibre/peek composites. Int J Impact Eng 23:519. https://doi.org/10.1016/s0734-743x(99)00101-3
74. Nebolsine PE, Humer ND, Harmon NF, Baker JR (1999) Statistical analysis of NRL 1964–1969 hypervelocity rodplate impact data and comparison to recent data. Int J Impact Eng 23:639. https://doi.org/10.1016/s0734-743x(99)00110-4
75. Condon JJ (1965) Rod lethality studies. NRL Report ALT-TR-65-18. Naval Research Laboratory, Washington DC
76. Condon J, Baker J (1967) Annual technical progress report on rod lethality studies. NRL Memorandum

77. Baker E, Templeton D (2011) Ballistics 2011: 26th international symposium, vol 2, DEStech Publications, Incorporated. https://books.google.co.in/books?id=L9oaDntTOvwC
78. Orphal DL (1999) Highly oblique impact and penetration of thin targets by steel spheres. Int J Impact Eng 23:687. https://doi.org/10.1016/s0734-743x(99)00114-1
79. Taylor EA, Herbert MK, Vaughan BA, Mcdonnell JA (1999) Hypervelocity impact on carbon fibre reinforced plastic/aluminium honeycomb: Comparison with whipple bumper shields. Int J Impact Eng 23:883. https://doi.org/10.1016/s0734-743x(99)00132-3
80. McMillan A (1967) Experimental investigations of simulated meteoroid damage to various spacecraft structures. National Aeronautics and Space Administration 915
81. Forrestal MJ, Piekutowski AJ (2000) Penetration experiments with 6061–T6511 aluminum targets and spherical-nose steel projectiles at striking velocities between 0.5 and 3.0 km/s. Int J Impact Eng 24(1):57. https://doi.org/10.1016/S0734-743X(99)00033-0
82. Palmieri D, Schäfer F, Hiermaier S, Lambert M (2001) Numerical simulation of non-perforating impacts on shielded gas-filled pressure vessels. Int J Impact Eng 26(1–10):591
83. Vlasov AS, Zilberbrand EL, Kozhushko AA, Kozschuk AI, Pugachev GS, Sinani AB (2001) Whipple shields against shaped charge jets. In 19th International Ballistics Symposium, p 1045
84. Ohtani K, Numata D, Kikuchi T, Sun M, Takayama K, Togami K (2006) A study of hypervelocity impact on cryogenic materials. Int J Impact Eng 33(1–12):555
85. Gongshun G, Baojun P, Wei Z, Yue H (2008) Crater distribution on the rear wall of AL-Whipple shield by hypervelocity impacts of AL-spheres. Int J Impact Eng 35(12):1541. https://doi.org/10.1016/j.ijimpeng.2008.07.028
86. Piekutowski AJ, Poormon K, Christiansen EL, Davis BA (2011) Performance of Whipple shields at impact velocities above 9 km/s. Int J Impact Eng 38(6):495
87. Ryan S, Christiansen E (2011) A ballistic limit analysis programme for shielding against micrometeoroids and orbital debris. Acta Astronaut 69(5–6):245
88. Jiyun Y, Kunbo X, Yabin J, Yan C, Yu L, Zizheng G, Jingjing Z (2011) The effects of hypervelocity impact on Whipple shield at cryogenic temperatures. Spacecraft Environment Engineering, p 4
89. Huang X, Ling Z, Liu ZD, Zhang HS, Dai LH (2012) Amorphous alloy reinforced Whipple shield structure. Int J Impact Eng 42:1. https://doi.org/10.1016/j.ijimpeng.2011.11.001
90. Zhen-Fei S, Jian-Heng Z, Shi-Cao Z, Jian-Jun M (2013) Evaluation of shielding performance of composite laminates under hypervelocity impact. Procedia Eng 58:496
91. Khatiwada S, Armada CA, Barrera EV (2013) Hypervelocity impact experiments on epoxy/ultra-high molecular weight polyethylene fiber composites reinforced with single-walled carbon nanotubes. Procedia Eng 58:4
92. Miller J, Bjorkman M, Christiansen E, Ryan S (2015) Analytic ballistic performance model of Whipple shields. Procedia Eng 103:389
93. Poniaev S, Bobashev S, Zhukov B, Kurakin R, Sedov A, Izotov S, Kulakov S, Smirnova M (2015) Small-size railgun of mm-size solid bodies for hypervelocity material testing. Acta Astronaut 109:162
94. Shield W, Hofmann DC, Hamill L, Christiansen E, Nutt S (2015) Hypervelocity impact testing of a metallic glass-stuffed Whipple Shield. Adv Eng Mat 17(9):1313
95. Liu M, Lissenden CJ, Wang Q, Su Z, Zhang Q, Long R (2017) Characterization of damage in shielding structures of space vehicles under hypervelocity impact. Procedia Eng 188:286. https://doi.org/10.1016/j.proeng.2017.04.486
96. Cha JH, Kim YH, Sathish Kumar SK, Choi C, Kim CG (2020) Ultra-high-molecular-weight polyethylene as a hypervelocity impact shielding material for space structures. Acta Astronaut 168:182. https://doi.org/10.1016/j.actaastro.2019.12.008
97. Poniaev SA, Bobashev SV, Zhukov BG, Kurakin RO, Sedov AI, Izotov SN, Kulakov SL, Smirnova MN (2015) Small-size railgun of mm-size solid bodies for hypervelocity material testing. Acta Astronaut 109:162. https://doi.org/10.1016/j.actaastro.2014.11.012
98. Olivieri L, Giacomuzzo C, Francesconi A, Stokes H, Rossi A (2020) Experimental characterization of multi-layer 3D-printed shields for microsatellites. J Space Safe Eng 7(2):125. https://doi.org/10.1016/j.jsse.2020.05.001
99. Wen XZ, Huang J, Li Y, Chen P, Jiang L, Long Y, Liu S (2016) Preliminary study on shielding performance of wood stuffed shield. Int J Impact Eng 91:94. https://doi.org/10.1016/j.ijimpeng.2015.12.006
100. Jing L, Lin J, Xuezhong W, Jie H, Qing L, Xuegang H, Sen L (2017) Primary study on shielding performance of aerogel/fiberglass composite stuffed in thermal insulation shield. Procedia Eng 204:429. https://doi.org/10.1016/j.proeng.2017.09.783
101. Fa-wei K, Jie H, Xue-zhong W, Xin L, Jing L, Qing L, Sen L (2018) Study on shield configuration stuffed with the integrated fabric layer and its bracing structure. Int J Impact Eng 121(June):191. https://doi.org/10.1016/j.ijimpeng.2018.06.005
102. Song ZF, Zhao JH, Zhao SC, Mo JJ (2013) Evaluation of shielding performance of composite laminates under hypervelocity impact. Procedia Eng 58:496. https://doi.org/10.1016/j.proeng.2013.05.057
103. Wells B (2006) Hypervelocity impact tests on coated thermoplastic films at cryogenic and elevated temperatures. Int J Impact Eng 33(1–12):855
104. Moon JB, Yoon SH, Kim CG (2016) High velocity impact test of a hybrid sandwich composite shield with unrestrained boundary fabric. Compos Struct 153:60
105. Fw Ke, Huang J, Xz Wen, Zx Ma, Liu S (2016) Test study on the performance of shielding configuration with stuffed layer under hypervelocity impact. Acta Astronaut 127:553
106. Huang X, Yin C, Huang J, Zhao XZ, Wu J, Liu S (2016) Hypervelocity impact of TiB2-based composites as front bumpers for space shield applications. Mater Design 97:473. https://doi.org/10.1016/j.matdes.2016.02.126
107. Guan GS, Zeng M, Li HJ (2016) Experimental investigation of multi-layer insulation effect on damage of stuffed shield by high-velocity impact. J Mater Eng 2016: 9
108. Wen XZ, Huang J, Li Y, Chen P, Jiang L, Long Y, Liu S (2016) Preliminary study on shielding performance of wood stuffed shield. Int J Impact Eng 91:94
109. Mespoulet J, Héreil P, Abdulhamid H, Deconinck P, Puillet C (2017) Experimental study of hypervelocity impacts on space shields above 8 km/s. Procedia Eng 204:508
110. Kim YH, Choi C, Sathish Kumar SK, Kim CG (2017) Hypervelocity impact on flexible curable composites and pure fabric layer bumpers for inflatable space structures. Compos Struct 176:1061. https://doi.org/10.1016/j.compstruct.2017.06.035
111. Kim YH, Choi C, Kumar SKS, Kim CG (2019) Behavior of dragon skin flexible metal bumper under hypervelocity impact. Int J Impact Eng 125:13. https://doi.org/10.1016/j.ijimpeng.2018.10.005
112. Fa-wei K, Jie H, Xue-zhong W, Xin L, Jing L, Qing L, Sen L (2018) Study on shield configuration stuffed with the integrated fabric layer and its bracing structure. Int J Impact Eng 121:191
113. Nam YW, Sathish Kumar SK, Ankem VA, Kim CG (2018) Multifunctional aramid/epoxy composite for stealth space hypervelocity impact shielding system. Compos Struct 193(March):113. https://doi.org/10.1016/j.compstruct.2018.03.046

114. Menglong L, Qiang W, Zhang Q, Renrong L, Fangsen C, Zhongqing S (2019) Hypervelocity impact induced shock acoustic emission waves for quantitative damage evaluation using in situ miniaturized piezoelectric sensor network. Chin J Aeronaut 32(5):1059
115. Xuezhong W, Jie H, Fawei K, Lin J, Jin L, Qiang S, Sen L (2019) Preliminary study on shielding performance of debris shield with the rear wall combining light materials and an aluminum plate. Int J Impact Eng 124:31
116. Cao W, Wang Y, Zhou P, Yang X, Wang K, Pang B, Chi R, Su Z (2019) Microstructural material characterization of hypervelocity-impact-induced pitting damage. Int J Mech Sci 163:105097
117. Zhang PL, Xu KB, Li M, Gong ZZ, Song GM, Wu Q, Cao Y, Tian DB, Yu ZJ (2019) Study of the shielding performance of a Whipple shield enhanced by Ti-Al-nylon impedance-graded materials. Int J Impact Eng 124:23. https://doi.org/10.1016/j.ijimpeng.2018.08.005
118. Zhang P, Gong Z, Tian D, Song G, Wu Q, Cao Y, Xu K, Li M (2019) Comparison of shielding performance of Al/Mg impedance-graded-material-enhanced and aluminum Whipple shields. Int J Impact Eng 126:101. https://doi.org/10.1016/j.ijimpeng.2018.12.007
119. Cha JH, Kim Y, Kumar SKS, Choi C, Kim CG (2020) Ultra-high-molecular-weight polyethylene as a hypervelocity impact shielding material for space structures. Acta Astronaut 168:182
120. Xuezhong W, Jie H, Zhaoxia M, Junyao Z, Fawei K, Jingui Q, Lin J, Jing L, Sen L (2020) Shielding performance of debris shield with separated rear wall. Int J Impact Eng 137:103446
121. Olivieri L, Giacomuzzo C, Francesconi A, Stokes H, Rossi A (2020) Experimental characterization of multi-layer 3D-printed shields for microsatellites. J Space Safe Eng 7(2): 125
122. Ren S, Zhang Q, Wu Q, Zheng YK, Lu Y, Liang H (2020) Influence of impact-induced reaction characteristics of reactive composites on hypervelocity impact resistance. Mater Design 192:108722. https://doi.org/10.1016/j.matdes.2020.108722
123. Poole LL, Gonzales M, French MR, Yarberry WA, Moustafa AR, Cordero ZC (2020) Hypervelocity impact of PrintCast 316L/A356 composites. Int J Impact Eng 136:103407. https://doi.org/10.1016/j.ijimpeng.2019.103407
124. Hofmann DC, Hamill L, Christiansen E, Nutt S (2015) Hypervelocity impact testing of a metallic glass-stuffed whipple shield. Adv Eng Mater 17(9):1313
125. Kumar SKS, Ankem VA, Kim Y, Choi C, Kim CG (2018) Polybenzimidazole (PBI) coated CFRP composite as a front bumper shield for hypervelocity impact resistance in low earth orbit (LEO) environment. Compos Res 31(3):83
126. Numata D, Ohtani K, Anyoji M, Takayama K, Sun M (2008) Experimental study of hypervelocity impacts at low temperatures. Shock Waves 18(3):169
127. Christiansen EL (1997) Evaluation of space station meteoroid/debris shielding materials report. Eagle Engineering Inc 87(163)
128. Schonberg WP, Darzi K (1992) Projectile shape and material effects in hypervelocity impact response of dual-wall structures. J Aerosp Eng 5(4):405
129. Ryan S, Thaler S, Kandanaarachchi S (2016) Machine learning methods for predicting the outcome of hypervelocity impact events. Expert Syst Appl 45:23
130. Qi C, Remennikov A, Pei LZ, Yang S, Yu ZH, Ngo TD (2017) Impact and close-in blast response of auxetic honeycomb-cored sandwich panels: experimental tests and numerical simulations. Compos Struct 180:161